Strong axial anisotropy of the magnetic penetration length in superconducting UPt_3

1998 J. Phys.: Condens. Matter 10 9791

(http://iopscience.iop.org/0953-8984/10/43/023)

J. Phys.: Condens. Matter **10** (1998) 9791–9798. Printed in the UK PII: S0953-8984(98)95426-1

Strong axial anisotropy of the magnetic penetration length in superconducting UPt_3

A Yaouanc†, P Dalmas de Réotier†, A Huxley†, J Flouquet†, P Bonville‡, P C M Gubbens§ and A M Mulders§

† Commissariat à l'Energie Atomique, Département de Recherche Fondamentale sur la Matière Condensée, F-38054 Grenoble Cédex 9, France

‡ Commissariat à l'Energie Atomique, Département de Recherche sur l'Etat Condensé, les Atomes et les Molécules, F-91191 Gif-sur-Yvette, France

§ Interfacultair Reactor Instituut, Delft University of Technology, 2629 JB Delft, The Netherlands

Received 6 June 1998, in final form 27 August 1998

Abstract. We report muon spin rotation measurements of the temperature dependence and anisotropy of the magnetic field penetration lengths in the heavy fermion superconductor UPt_3. We observe a strong axial anisotropy. At 0.05 K we obtain for the penetration length parallel and perpendicular to the c axis $\lambda_c = 4260$ (150) Å and $\lambda_a = 6040$ (130) Å, respectively. $\lambda_a^{-2}(T)$ at low temperatures excludes a superconducting order parameter in the B phase with only a line of nodes in the equatorial plane of the Fermi surface. The combined analysis of $\lambda_c^{-2}(T)$ and $\lambda_a^{-2}(T)$ measured in the B phase favours an hybrid order parameter with point nodes at the poles and a line of nodes at the equatorial plane. The A phase is characterized by a larger density of nodes than the B phase.

While the occurrence of two low field superconducting phases (the low temperature B phase and the high temperature A phase with critical temperature T_{C-} and T_{C+}, respectively) in the hexagonal heavy fermion UPt_3 is now well established [1, 2], the determination of the topology of the superconducting order parameter (Δ) has proved to be a rather difficult problem. The spatial symmetry of Δ in the A phase is unknown. Transport measurements [3–5] and point-contact spectroscopy [6, 7] have shown that Δ is anisotropic in the B phase. It has a line of nodes in the basal plane. But extracting quantitative information is difficult because the transport measurements require for their understanding a knowledge of the mean free path of the thermally excited quasiparticles. Measurements of a static property such as the magnetic penetration length λ should be easier to interpret. In fact such measurements have already been performed using the muon spin rotation (μSR) technique on unannealed samples [8]. But since the reported anisotropy of λ is much smaller than expected, the node structure of Δ inferred from these measurements could be unreliable. The physical properties of UPt_3 are well known to be extremely dependent on the sample quality. In addition, we note that the data analysis of Broholm *et al* [8] has been disputed [9]. These facts motivated our new μSR study.

The μSR technique is unique in that it is not influenced by surface effects and gives absolute values for λ. A magnetic field B_{ext} applied along the z axis, perpendicular to the initial muon spin polarization, generates a flux lattice. The muon spins evolve in it until

0953-8984/98/439791+08$19.50

the muons decay [10–12]. The decay positron is emitted preferentially along the final muon spin direction; by collecting positrons, we reconstruct the time dependence of the muon spin depolarization function $P(t)$ which reflects the distribution of fields experienced by the muons. The root mean square of this distribution is [13, 14]

$$\Delta_{\rm v} = 6.092 \times 10^{-2} f(B_{\rm ext}/B_{\rm c2}) \frac{\Phi_0}{\lambda_x \lambda_y} \tag{1}$$

where $B_{\rm c2}$ is the upper critical field, Φ_0 the quantum of flux ($\Phi_0 = 2.07 \times 10^{-15}$ T m^2) and λ_i the penetration length along the i axis. The universal function f describes the effect of the finite size of the vortex cores [14].

$\lambda_i^{-2}(T)$ factorizes as $\lambda_i^{-2}(T) = \lambda_i^{-2}(0)\rho_i^s(T)$ where $\rho_i^s(T)$ is the normalized superfluid density in the i direction [15]. If Δ has a high density of nodes in the i direction, the normal quasiparticles are easily excited and $\lambda_i^{-2}(T)$ decreases rapidly with increasing temperature. Therefore the study of the anisotropy and temperature dependence of λ^{-2} is an efficient method to map out the location and characteristics of nodes.

The μSR measurements were performed at the MuSR spectrometer [16] of the ISIS facility (Rutherford Appleton Laboratory, UK). We used the two high quality crystals described in a recent letter [17]. Their high quality is demonstrated by the specific heat (the two superconducting temperatures are well defined as seen in figure 3) and the residual resistivities at low temperature ($\rho_c(0) = 0.17$ $\mu\Omega$ cm and $\rho_b(0) = 0.54$ $\mu\Omega$ cm [5]) are among the lowest ever reported. The geometry of the experiment was such that one sample was studied with $B_{\rm ext}$ parallel either to c or a and the second sample with $B_{\rm ext}$ parallel either to a or a^*. The measurements with $B_{\rm ext} \| a$ could therefore be done with the two samples and gave similar results. In each case $B_{\rm ext}$ was applied parallel to the sample disc, minimizing the diamagnetization effect. We took $B_{\rm ext} = 18$ mT. The measurements were performed down to $T/T_{\rm C-} \lesssim 1/10$. We paid attention to perform the field cooled measurements in a state of thermal equilibrium: a target temperature was very slowly reached from above (within $\sim$15 min). The positrons were recorded with 32 detectors [16]. The data of the neighbouring detectors were added four by four giving rise to eight effective sets of data, i.e. to eight spectra. In figure 1 we present two spectra taken at different temperatures. All the spectra are well analysed by the sum of two functions

$$a P(t) = a_{\rm s} \exp\left(\frac{-\gamma_\mu^2 \Delta_{\rm tf}^2 t^2}{2}\right) \cos(\gamma_\mu \langle B \rangle t + \phi) + a_{\rm bg} \cos(\gamma_\mu B_{\rm ext} t + \phi). \tag{2}$$

The first function describes the μSR response of the sample and the second accounts for the muons stopped outside the sample. As most of these muons stop in the silver sample holder and cryostat windows, the second component is weakly damped. γ_μ is the muon gyromagnetic ratio ($\gamma_\mu = 851.6$ Mrad s^{-1} T^{-1}), $\gamma_\mu \Delta_{\rm tf}$ the damping rate, $\langle B \rangle$ the mean field in the sample, ϕ an initial phase which depends on the detector location. The low temperature measurements allowed us to determine the asymmetry of the background, $a_{\rm bg}$. We found $a_{\rm bg} = 0.09$. It was then taken as a fixed parameter at high temperature. All the other parameters were free in the fits. We had $a_{\rm s} \simeq 0.125$. For a given experimental condition, the parameters of the eight spectra were averaged to yield the final parameters [18]. We do see a large relative frequency shift at low temperature which reflects the diamagnetic response: relative to the frequency shift above $T_{\rm C+}$, the frequency shift at 0.05 K is $\sim$2.5% and 0.5% for $B_{\rm ext}$ applied perpendicular and parallel to the c axis, respectively.

In figure 2 we present $\Delta_{\rm tf}(T)$ for three different directions of $B_{\rm ext}$ relative to the crystal axes. Whereas in the paramagnetic state our results are consistent with published data [8, 19], in the B phase they drastically differ, reflecting the effect of the sample quality

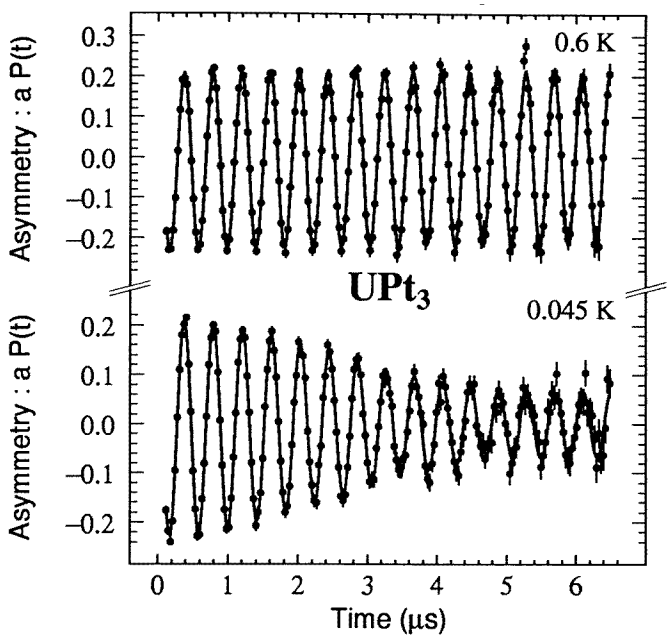

Figure 1. Examples of μSR spectra recorded on UPt_3. The field distribution due to the vortex lattice induces a strong damping of the oscillations at low temperature. Solid lines are from fits described in text.

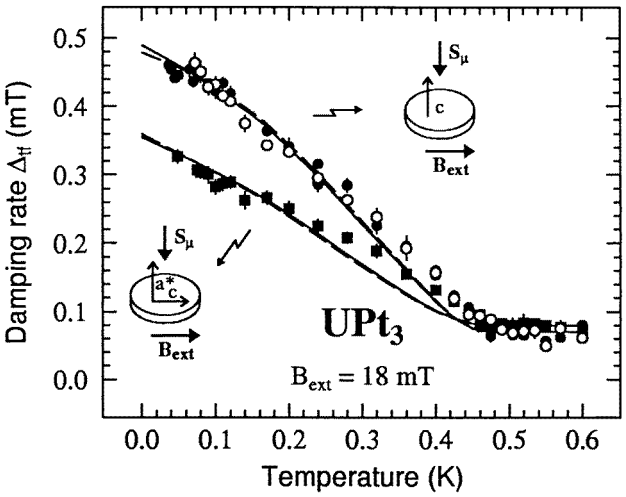

Figure 2. Temperature dependence of the transverse field width Δ_{tf} measured in field cooling on UPt_3 for three different directions of the applied field, B_{ext}, relative to the crystal axes. The axial anisotropy is strong and the planar anisotropy negligible (open and closed circles correspond to B_{ext} parallel to a and a^*, respectively). The dashed and solid lines are from fits to models I and II, respectively.

on the vortex field distribution. We observe a stronger axial anisotropy and larger field distributions, i.e. smaller penetration lengths. There is no planar anisotropy.

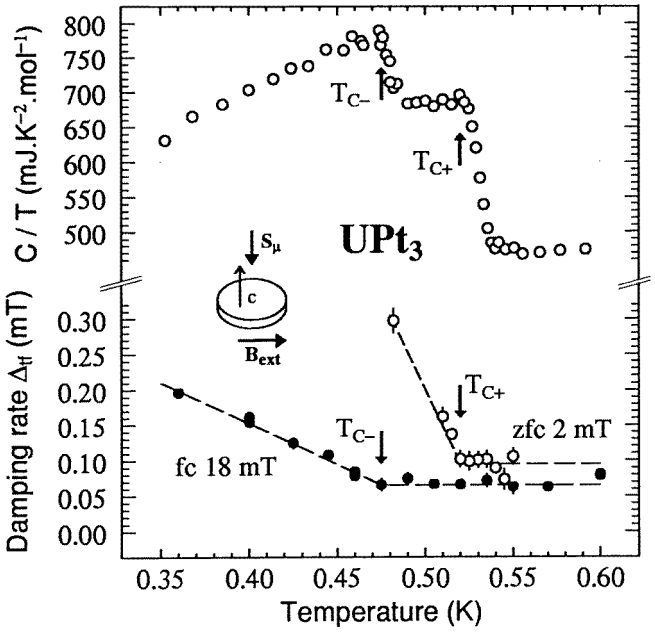

Figure 3. Zero-field specific heat and Δ_{tf} for $B_{ext} \| a^*$ near 0.5 K. The open and closed circles correspond to spectra recorded at 2 mT using a zero-field cooled (zfc) procedure and at 18 mT in field cooling (fc) experiments, respectively. The high temperature level of the zfc data is higher than for fc data because the zfc spectra have been recorded using auxiliary coils, the field of which is not very homogeneous. The dashed lines are guides to the eyes. It is rewarding that the two superconducting temperatures as determined by specific heat and μSR measurements are consistent.

In figure 3 we compare the temperature dependence of the zero-field specific heat C (divided by the temperature) and the zero-field cooling (zfc) and field cooling (fc) damping rates (in field units) for temperatures near 0.5 K and $B_{ext} \parallel a^*$. The two superconducting temperatures as determined by specific heat and μSR are consistent. The same agreement is found for B_{ext} parallel to a and c. As noticed previously [19] the zfc and fc measurements clearly distinguish the two superconducting temperatures. The fc measurements do not detect the vortex lattice field distribution of the A phase. This is a fingerprint of the extremely large λ value, i.e. of the presence of more quasiparticles in the A phase than would be present if the B phase extended up to the same temperature. We estimate that λ is larger than $\approx$1.6 μm. The difference between the zfc and fc damping rates may reflect the effect of flux pinning on the zfc measurements [20].

We have modelled the signal from the sample by a product of a Gaussian and an oscillating function. Although this is certainly a rough approximation, it should yield reliable estimates of the temperature dependence of the penetration lengths [21] and their anisotropy. We have not attempted to determine the field distribution lineshape, and therefore to obtain more information than simply the penetration length, because the background signal is too large to extract reliable lineshapes characterized by relatively small widths. Recently Lee *et al* [22] have managed to observe such types of lineshape at the ISIS facility. But for recording their data they only needed a helium cryostat which has a background signal drastically reduced compared to the dilution cryostat.

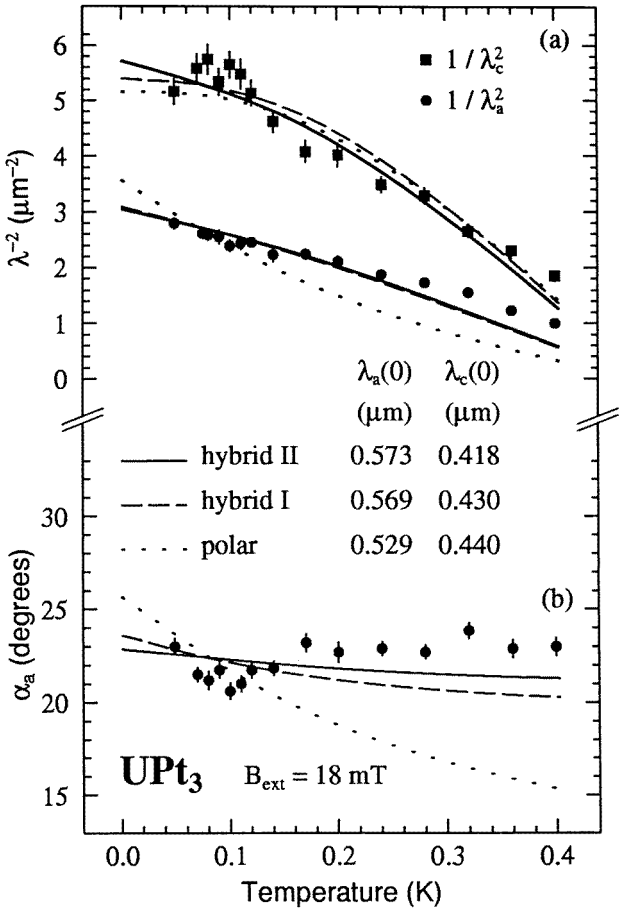

Figure 4. Temperature dependence of parameters deduced from the analysis of the μSR data. (a) λ_c^{-2} (squares) and λ_a^{-2} (circles). (b) Opening angle α_a (= α_{a*}) of the vortex lattice for the field applied in the basal plane. The data are presented for $T \leqslant 0.4$ K. Lines give the predictions of models described in the text. For the polar state $\Delta_0 = 1.17$ [15].

Above T_{C-} the damping is only due to the ^{195}Pt nuclear magnetic moments characterized by a root mean square Δ_n. Therefore $\Delta_v = (\Delta_{tf}^2 - \Delta_n^2)^{1/2}$. Then, using the data of figure 2 and equation (1), we compute λ_i^{-2}. Since B_{c2} is not changing drastically with temperature for $T \leqslant 0.4$ K [23], $f(B_{ext}/B_{c2})$ varies only from 0.84 and 0.81 at 0.4 K to 0.92 and 0.90 at 0.2 K for B_{ext} perpendicular and parallel to c, respectively. At lower temperature it is temperature independent. Therefore the extrapolation of λ_i to $B_{ext} = 0$ does not modify its low temperature dependence. $\lambda_i^{-2}(T)$ are presented in figure 4. The mean free path l being very large relative to the coherence length ξ_0 ($l \geqslant 5000$ Å and $\xi_0 \sim 150$ Å; see [5]), we do not correct λ_a and λ_c for finite mean free path. At 0.05 K we obtain $\lambda_c = 4260$ (150) Å and $\lambda_a = 6040$ (130) Å, in reasonable agreement with estimates from neutron diffraction ($\lambda_c = 4220$ (90) Å and $\lambda_a = 7150$ (150) Å [24]) and at variance with previous μSR data ($\lambda_c = 7070$ (30) Å and $\lambda_a = 7820$ (30) Å [8]). The agreement between the neutron and our μSR results justifies the model used for the μSR data analysis. We derive the lower critical

field $B_{c1} = \Phi_0 \ln(\lambda/\xi)/(4\pi\lambda^2) \approx 1.7$ mT and 2.5 mT for $B_{\rm ext}$ parallel and perpendicular to c. $B_{\rm ext}$ was therefore well above B_{c1}, a requirement for the applicability of our analysis.

Our data analysis supposes that the increase of the field inhomogeneity in the B phase is only due to the flux line lattice. This is justified since the upper bound on a possible internal magnetic field at the muon site due to the Cooper pairs is very small: 3 μT [17]. Even if an internal field of 10 μT were really induced by the Cooper pairs as measured by Luke *et al* [9], this field would still be much smaller that the field due to the flux line lattice (see figure 2). In the past it has been suggested that this lattice can not be at the origin of the measured field inhomogeneity since the inhomogeneity is strongly field dependent [9]. This argument is not valid [14].

Minimizing the free energy of the anisotropic London model with respect to the opening angle α_z of the vortex lattice in the reciprocal lattice, a closed form expression is derived: $\tan\alpha_z = \lambda_x/(\sqrt{3}\lambda_y)$ [25]. Therefore we can estimate α_z from the penetration length anisotropy. As a first consequence, since there is no planar anisotropy, the flux lattice for $B_{\rm ext}\|c$ is triangular. As a second consequence, the measured axial anisotropy gives us the possibility to determine α_a ($=\alpha_{a^*}$) characterizing the flux lattice for $B_{\rm ext} \perp c$. From the μSR measurements it is not possible to choose between the following two choices: λ_x is either λ_a or λ_c. But since neutron diffraction indicates $\alpha_a < 30^\circ$, the appropriate choice is $\lambda_x = \lambda_c$. In figure 4(b) we present $\alpha_a(T)$. The agreement between the low temperature α_a value as deduced from μSR here and by neutron ($\approx 19^\circ$ [24]) is rewarding. Note that the temperature dependence of the opening angle has already been presented in a recent review [11], but with a different definition of the angle. In this report we use the same definition as in [24].

For the quantitative analysis of $\lambda_i^{-2}(T)$ we need to specify the shape of the Fermi surface. For simplicity we model it with a single ellipsoid of anisotropy mass ratio r_N ($r_N = m_a/m_c$). Referring to the literature [1, 2] we write $|\Delta(\theta,\varphi,T)| = \Delta_0(T)g(\theta,\varphi)$ where θ and φ are the polar and azimuthal angle, respectively. We first consider the B phase. It is well established that Δ has at least a line of nodes in the basal plane [4]. As a first step we test whether the single line of nodes hypothesis is consistent with our data. Thus we write $g_B = Y_{10}$ where Y_{10} is an ellipsoidal harmonic. As shown in figure 4(a) the polar symmetry cannot explain $\lambda_a^{-2}(T)$ at low temperatures. Therefore Δ has nodes at the poles of the Fermi surface: it must be hybrid. Following Norman and Hirschfeld [26] we write g_B as a sum of Y_{lm} normalized such that Δ_0 is the maximum of Δ. We consider two simple gaps: $g_B = Y_{21} + \epsilon Y_{41}$ and $g_B = Y_{32} + \epsilon Y_{52}$ for model I and II, respectively. The Ginzburg–Landau expansion of symmetry E_{1g} (E_{2u}) [1, 2] yields $g(\theta,\varphi)$ given by model I (II). If the mixing parameter $\epsilon = 0$, Δ vanishes linearly (quadratically) with θ at the poles for model I (II). $\Delta(\theta)$ near $\theta = \pi/2$ is the same for the two models. We use the weak-coupling gap interpolation formula $\Delta_{0,\nu}(T) = \Delta_0 \tanh(a\sqrt{T_{C\nu}/T - 1})$ with $T_{C\nu} = T_{C-} = 0.475$ K. The parameters a and Δ_0 are only weakly dependent on the symmetry of Δ and on r_N [15]. We take $a = 1.7$ and $\Delta_0 = 1.0$ K. Resistivity measurements suggest $r_N = 1.65$ [27].

In figures 2 and 4(a) we compare our data with the model predictions. The curves are the results of combined fits of all the data of figure 2. The two hybrid models describe reasonably well the data at low temperatures. The best agreement is found for $\epsilon = -0.1$. On the other hand, at high temperatures, both predict lower superfluid density than observed. The strongest discrepancy occurs for $\lambda_a^{-2}(T)$ at $T \gtrsim T_{C-}/2$. The high temperature misfit is not reduced by taking into account the interference between the two components of Δ [28]. We have attempted to improve the fits by adjusting all the parameters ($\lambda_a^{-2}(0)$, $\lambda_c^{-2}(0)$, ϵ, r_N, a, Δ_0). Keeping these parameters in reasonable bounds ($-0.5 \leqslant \epsilon \leqslant 0$, $0 \leqslant r_N \leqslant 2.5$,

$1.5 \leqslant a \leqslant 1.9$, $0.85 \leqslant \Delta_0 \leqslant 1.15$), we have not found a parameter set yielding a better description than the ones initially obtained. Interestingly, the analysis shows that ϵ cannot have an appreciable positive value. We do not understand the origin of the misfit which is clearly reflected in figure 4(b).

We have estimated λ at 0.48 K for the A phase assuming the hybrid models with $\epsilon = 0$. The g_A function is then equal to $\sin\theta\cos\theta\cos\varphi$ and $\sin^2\theta\cos\theta\cos 2\varphi$ for models I and II, respectively. We have used $\Delta_{0,+}(T)$ with $T_{C+} = 0.520$ K, $r_N = 1$ and Δ_0, a, $\lambda_c(0)$ and $\lambda_a(0)$ at their values determined for the B phase. For model I we find $\lambda_i = 2.1$, 3.6 and 1.6 μm for $i = a$, a^* and c, respectively. The same computation for model II gives $\lambda_c = 1.8$ and $\lambda_a = 2.5$ μm. All these values are consistent with the experimental bounds.

In summary, we have mostly probed the B phase. We have discovered a strong axial anisotropy of the penetration length tensor in that phase. We did not detect any basal plane anisotropy. We have measured as a function of the temperature the angle characterizing the vortex lattice for B_{ext} in the basal plane. The low-temperature dependence of the penetration lengths indicates that the order parameter has certainly an appreciable density of nodes at the poles of the Fermi surface. Our data do not allow us to select between the considered hybrid models. Astonishingly they overestimate the penetration length at high temperatures. Our analysis is based on the hypothesis that the Fermi surface is a single ellipsoidal surface. This is certainly an oversimplification. Since we have modelled the lineshape by a Gaussian function, there is as well the possibility that this model does take into account a possible change of lineshape as the temperature increases. To investigate this last point, a proper lineshape is required. This may not be feasible because of the relatively large background in the dilution cryostat at ISIS. We have inferred that the node density in the A phase is significantly enhanced as compared to the B phase as predicted by the hybrid models.

Acknowledgments

We thank V P Mineev for useful discussions. The researchers from the Netherlands acknowledge support from the Dutch Scientific Organization (NWO). We thank the ISIS facility crew for the excellent working conditions and A D Taylor for his support. The μSR measurements were partly supported by the Commission of the European Community through the Large Installations Plan.

References

[1] Sauls J A 1994 *Adv. Phys.* **43** 113
[2] Heffner R H and Norman M R 1996 *Comment Condens. Matter Phys.* **17** 361
[3] Shivaram B S, Jeon Y H, Rosenbaum T F and Hinks D G 1986 *Phys. Rev. Lett.* **56** 1078
[4] Lussier B, Ellman B and Taillefer L 1994 *Phys. Rev. Lett.* **73** 3294
Lussier B, Ellman B and Taillefer L 1996 *Phys. Rev.* B **53** 5145
[5] Suderow H, Brison J P, Huxley A and Flouquet J 1998 *Phys. Rev. Lett.* **80** 165
[6] Goll G, v Höhneysen H, Yanson I K and Taillefer L 1993 *Phys. Rev. Lett.* **70** 2008
[7] De Wilde Y, Heil J, Jansen A G M, Wyder P, Deltour R, Assmus W, Menovsky A, Sun W and Taillefer L 1994 *Phys. Rev. Lett.* **72** 2278
[8] Broholm C, Aeppli G, Kleiman R N, Harshman D R, Bishop D J, Bucher E, Williams D Ll, Ansaldo E J and Heffner R H 1990 *Phys. Rev. Lett.* **65** 2062
[9] Luke G M *et al* 1991 *Phys. Lett.* **157A** 173
[10] Schenck A and Gygax F N 1995 *Handbook of Magnetic Materials* vol 9, ed K H J Buschow (Elsevier)
[11] Dalmas de Réotier P and Yaouanc A 1997 *J. Phys.: Condens. Matter* **9** 9113
[12] Amato A 1997 *Rev. Mod. Phys.* **69** 1119
[13] Barford W and Gunn J M F 1988 *Physica* C **156** 515
[14] Yaouanc A, Dalmas de Réotier P and Brandt E H 1997 *Phys. Rev.* B **55** 11 107

[15] Gross F, Chandrasekhar B S, Einzel D, Andres K, Hirschfeld P J, Ott H R, Beuers J, Fisk Z and Smith J L 1986 *Z. Phys.* B **64** 176
Gross-Alltag F, Chandrasekhar B S, Einzel D, Hirschfeld P J and Andres K 1990 *Z. Phys.* B **82** 243
[16] Eaton G H, Scott C A and Williams W G 1994 *Hyperfine Interact.* **85** 1099
[17] Dalmas de Réotier P, Huxley A, Yaouanc A, Flouquet J, Bonville P, Imbert P, Pari P, Gubbens P C M and Mulders A M 1995 *Phys. Lett.* **205A** 239
[18] Dalmas de Réotier P, Yaouanc A, Eaton G H and Scott C A 1990 *Hyperfine Interact.* **65** 1113
[19] Luke G M, Keren A, Le L P, Wu W D, Uemura Y J, Bonn D A, Taillefer L and Garrell J D 1993 *Phys. Rev. Lett.* **71** 1466
[20] Wu W D, Keren A, Le L P, Luke G M, Sternlieb B J, Uemura Y J, Seaman C L, Dalichaouch Y and Maple M B 1993 *Phys. Rev.* B **47** 8172
[21] Sonier J E *et al* 1994 *Phys. Rev. Lett.* **72** 744
[22] Lee S L, Pratt F L, Blundell S J, Aegerter C M, Pattenden P A, Chow K H, Forgan E M, Sasaki T, Hayes W and Keller H 1997 *Phys. Rev. Lett.* **79** 1563
[23] Keller N, Brison J P, Lejay P, Tholence J L, Huxley A, Schmidt L, Buzdin A and Flouquet J 1995 *Physica* B **206** 568
[24] Kleiman R N, Broholm C, Aeppli G, Bucher E, Stücheli N, Bishop D J, Clausen K N, Mortensen K, Pedersen J S and Howard B 1992 *Phys. Rev. Lett.* **69** 3120
[25] Kogan V G 1981 *Phys. Lett.* **85A** 298
[26] Norman M R and Hirschfeld P J 1996 *Phys. Rev.* B **53** 5706
[27] Huxley A D, Suderow H, Brison J P and Flouquet J 1995 *Phys. Lett.* **209A** 365
[28] For a 2D representation we have $|\Delta(\theta, \varphi, T)| = \cos\theta \sin^{\tau}\theta[\Delta_{0,+}(T)\cos(\tau\varphi) + \mathrm{i}\Delta_{0,-}(T)\sin(\tau\varphi)]$ with $\tau = 1$ and 2 for model I and II, respectively.